JOURNAL OF PETROLEUM AND GEOTHERMAL TECHNOLOGY
ISSN: 2723-0988, e-ISSN: 2723-1496
Vol. 6 No. 2 2025

Waterflood and Polymer Injection Design for New Target Reservoir based on Injection Pattern Optimization, Injection Rate Sensitivity, and Injection Pressure Sensitivity

Fransiscus Asisi Lugas Ariobimo [1*], Boni Swadesi [1], H. KRT Nur Suhascaryo [1]
[1] Petroleum Engineering, Universitas Pembangunan Nasional Veteran Yogyakarta
* corresponding email: fransiscuslugas@gmail.com

ABSTRACT

Field "X" is in Tabalong Regency, South Kalimantan, and is operated by Pertamina Hulu Indonesia Zona 9. The peak primary production occurred in March 1963, reaching 47,963 BOPD. Full-scale waterflood implementation with a staggered line-drive injection pattern began in January 1995, and the peak secondary production occurred in January 1999 at 10,095 BOPD. This study was conducted using a dynamic model that had undergone initialization validation and history matching. The assessment of polymer injection pattern candidates was carried out through a screening stage based on screening criteria and reservoir property analysis to determine patterns that could be prioritized as pilot areas for an optimal polymer injection scenario in Zone B. Pattern analysis criteria were based on movable remaining oil saturation, movable remaining oil in place, pattern area, and average transmissibility, evaluated for the Zone B reservoir under post-waterflood conditions. Sensitivity analyses on water injection rate and injection pressure were then performed to obtain the optimum waterflood injection scenario. After optimizing the injection pattern and determining the optimum waterflood injection scenario, polymer input parameters were applied to the model, followed by sensitivity analyses on polymer injection rate and pressure to obtain the optimum polymer injection scenario for Zone "B" of Field "X By the end of the production forecast in January 2066, the optimum waterflood injection scenario at the end of the production forecast provides an incremental oil gain of 1.5 MMSTB with an incremental recovery factor of 2.19% relative to OOIP, while the combination of optimum waterflood and polymer injection at the end of the production forecast provides an incremental oil gain of 2.14 MMSTB with an incremental recovery factor of 3.13% relative to OOIP; demonstrating improved sweep efficiency, oil bank formation, and effective mobilization of residual oil across Zone B.

Keywords: injection flow rate; injection pressure; waterflooding; polymer flooding; screening criteria

I. INTRODUCTION

Indonesia's oil fields are dominated by mature fields that were discovered during the Dutch East Indies colonial era. As oil demand continues to increase, various studies and technologies have been developed with the aim of optimizing the recovery factor. One method that can be applied is Chemical Enhanced Oil Recovery (EOR) injection, one of which is polymer injection. Polymers are used to increase the viscosity of the injected water to minimize viscous fingering effects within the rock pores, allowing the polymer-mixed water to displace oil more effectively toward production wells.

The assessment process for injection pattern candidates was carried out through a screening stage based on screening criteria and an analysis based on reservoir properties to determine patterns that can be prioritized as pilot areas for the optimum polymer injection scenario in Zone B. The main parameters in designing polymer injection are movable oil saturation, movable remaining oil in place, and average transmissibility (Taber. J.J., et al., 1996). Liang, et al. (2018) stated that movable remaining oil in place, as a function of movable oil saturation, area, reservoir thickness, and porosity, is weighted twice as large as that of movable oil saturation itself. Dong et al. (2008), in their research in the Daqing Oilfield, stated that injection pattern area, as a function of well spacing, indicates that smaller injection pattern areas result in better oil recovery than larger injection pattern areas, and that pattern shape does not have a significant effect on oil recovery.

Field X has four main oil-producing reservoirs, namely Zones A, B, C, and D. Chemical EOR injection testing and pilot testing have been conducted in Zones A and C, while Zones B and D still use waterflooding to enhance oil production. In 2020, a coreflooding test of FP3230S polymer at 2000 ppm, totaling 1 PV, was conducted in the laboratory using stacked native core samples from Zone A. By applying a chemical EOR data input analogy based on the study by Tay, et al. (2015) regarding the effect of reservoir brine salinity on chemical adsorption, and the study by Yerramilli, et al. (2013) regarding the effect of reservoir brine salinity on polymer viscosity; an optimum polymer injection scenario was modeled to enhance oil recovery from Zone B. The research results and laboratory tests conducted for the Zone A reservoir were then analogized and adjusted to design the chemical EOR injection scenario for Zone B of Field X.

The purpose of this study is to determine a polymer CEOR injection plan that is suitable for Zone B as a new target reservoir to enhance oil recovery. The objectives of this study are to:

1. Describe the target reservoir based on rock and fluid properties (crude oil gravity and brine salinity).
2. Determine polymer injection pattern candidates based on ranking from the integration of screening-criteria parameters.
3. Determine the optimum waterflood and polymer injection operational design by conducting sensitivity analyses on injection pressure and injection rate.

II. METHODS

The methodology used in this study consisted of several steps through qualitative and quantitative analysis to achieve the thesis objective. The problem is limited to analyzing optimum waterflood and polymer flooding scenario indicated by increments of oil recovery, without considering economic analysis. The proposed strategy includes adding 5 new injection wells.

This research begins from the objective, which to examine polymer injection pattern candidates based on ranking from the integration of screening-criteria parameters, and determining the optimum polymer injection operational design by conducting sensitivity analyses on injection pressure and injection rate. After determining the purpose of this study, data collection and processing are required to create a pilot model and a full-scale model.

Literature reviews are undertaken to improve the information on the effects of brine salinity to polymer adsorption and viscosity, also on the analyses of the polymer flooding screening criteria to examine polymer injection pattern candidates. After data processing and literature reviews have been conducted, a dynamic model was prepared and validated. After the valid model is available, polymer characteristics tailored for Zone B are incorporated into the model. Based on the objective, analysis each for optimum waterflood and polymer injection scenario will be conducted through sensitivity analyses on the injection rate and pressure. Total production rate is adjusted according to total injection rate. Finally, a thorough analysis is conducted to see the result. The thesis then can be concluded, and a recommendation has been made for future research.

III. RESULTS AND DISCUSSION

Field “X” is in Tabalong Regency, South Kalimantan, and is operated by Pertamina Hulu Indonesia Zona 9. The peak primary production occurred in March 1963, reaching 47,963 BOPD. Full-scale waterflood implementation with a staggered line-drive injection pattern began in January 1995, and the peak secondary production occurred in January 1999 at 10,095 BOPD.

Field X has four main oil-producing reservoirs, namely Zones A, B, C, and D. Chemical EOR injection testing and pilot testing have been conducted in Zones A and C, while Zones B and D still use waterflooding to enhance oil production. All reservoirs are driven by weak water drive in combination with water injection. Zone B has 84 active production wells, and 22 active injection wells at June 2022, in which oil production reached 360 BOPD and water injection is at 7256 BWIPD. Last recorded water cut value is at 95.5%.

Based on existing core analysis, Zone B has an average porosity of 16%, 14.21 mD of horizontal permeability, 33% of connate water saturation, 28% of residual oil saturation, 100% of permeability relative to oil at connate water saturation, and 30% of permeability relative to water at residual oil saturation. From routine core analysis, Zone B could be classified into 5 rock regions/rock types, based on its flow zone indicator (FZI) distribution. Table 1 contains fluid saturation and oil-water relative permeability end-point.

Table 1. Fluid Saturation and Oil-Water Relative Permeability End-Point

Rock Type	FZI Range	FZI	Porosity, fraction	Perm., mD	Swc, fraction	Sor, fraction	Kro @ Swc, fraction	Krw @ Sor, fraction
RT-1	>1.92	2.58	0.18	49.19	0.28	0.30	1	0.35
RT-2	1.21 - 1.92	1.46	0.17	28.39	0.31	0.29	1	0.32
RT-3	0.74 – 1.21	0.95	0.17	9.77	0.34	0..28	1	0.29
RT-4	0.27 – 0.74	0.52	0.15	2.24	0.38	0.27	1	0.26
RT-5	<0.27	0.24	0.16	0.44	0.43	0.25	1	0.22
AVG		1.03	0.16	14.21	0.33	0.28	1	0.30

JOURNAL OF PETROLEUM AND GEOTHERMAL TECHNOLOGY
ISSN: 2723-0988, e-ISSN: 2723-1496
Vol. 6 No. 2 2025

Coreflooding test used stacked native core sample from Zone A, which had 23.03% porosity, permeability 206.87 mD, 63.5% water saturation, effective pore volume of 26.85 cc, and initial oil-in-place (IOIP) as many as 9.8 cc. When injected with water 2 PV, then FP3230S polymer 2000 ppm 1 PV, and lastly post-flush 3 PV; incremental oil recovery factor from polymer flood reached 3.67% relative to IOIP, and after post-flush was injected the total system incremental oil recovery factor reached 9.18%. This would be the benchmark for the Zone B polymer flood optimization results. Core sample initial condition is shown in Figure 1, coreflood simulation history matching is shown in Figure 2, parameters adjusted for simulation is shown in Figure 3, and the summary of polymer coreflooding is shown in Figure 4.

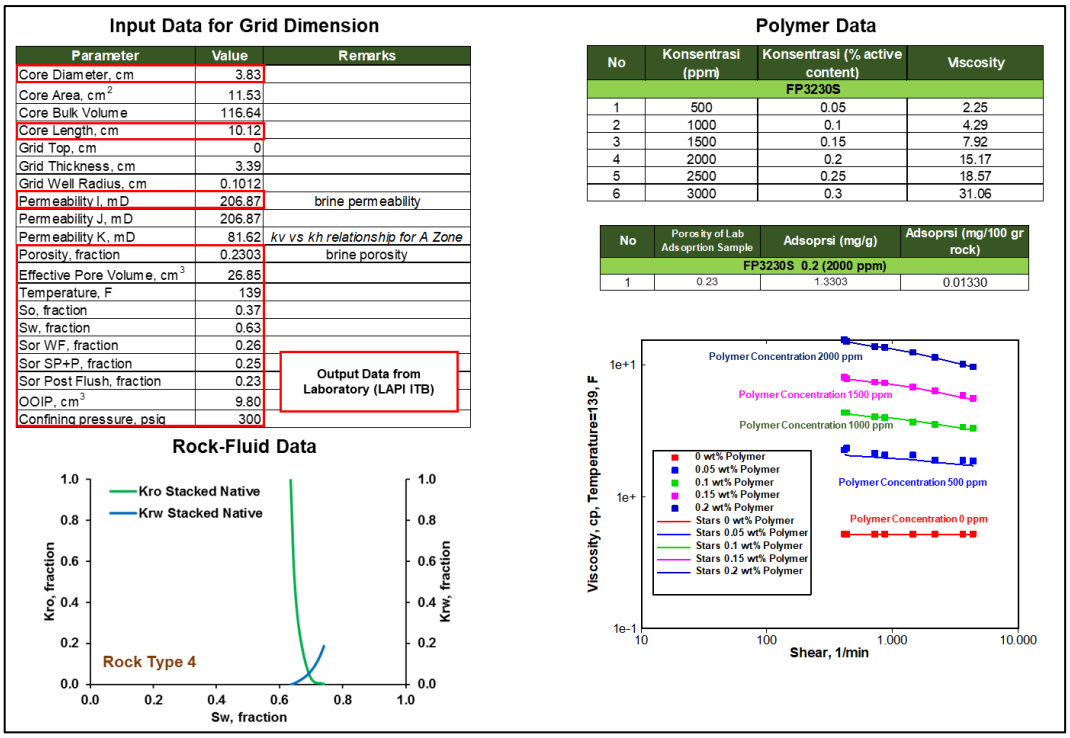

Figure 1. Stacked Native Core Sample Initial Conditions for FP3230S 2000 ppm 1.0 PV Injection

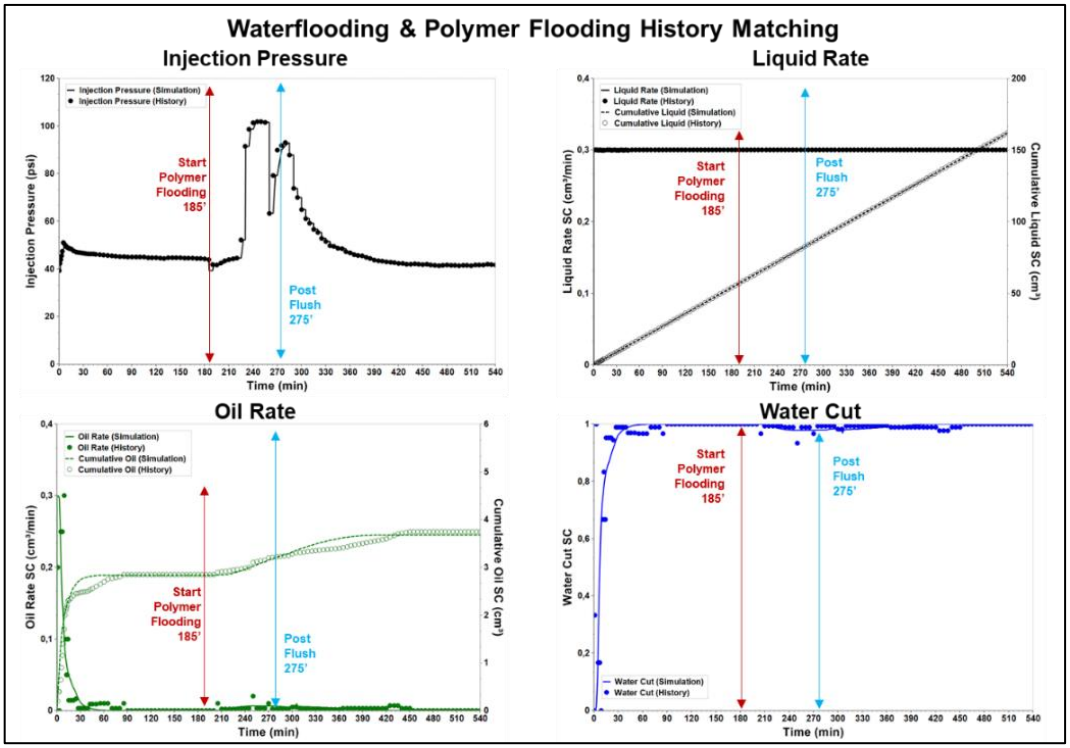

Figure 2. Coreflood Simulation History Matching Results for FP3230S 2000 ppm 1.0 PV Injection

JOURNAL OF PETROLEUM AND GEOTHERMAL TECHNOLOGY
ISSN: 2723-0988, e-ISSN: 2723-1496
Vol. 6 No. 2 2025

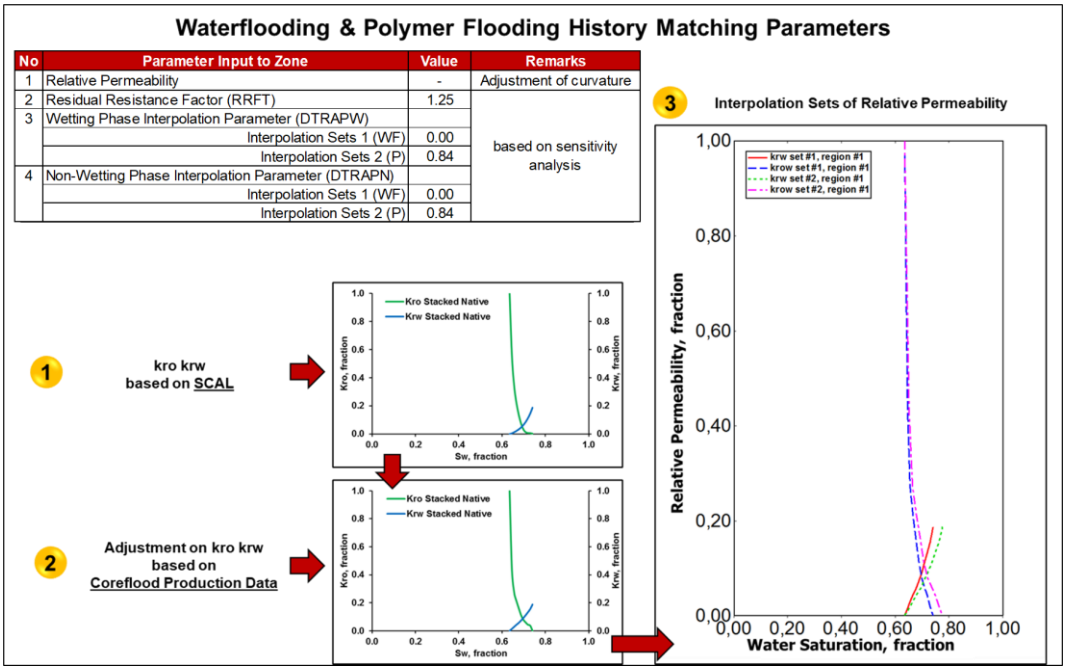

Figure 3. Parameters Adjusted for Coreflood History Match Simulation FP3230S 2000 ppm 1.0 PV Injection

Waterflood History Matching

Waterflooding			
Parameter	History	Simulation	% Difference
Cumulative Liquid, cm^3	54.00	54.00	0.00
Cumulative Oil, cm^3	2.85	2.84	0.49
Cumulative Water, cm^3	51.15	51.16	0.03

Polymer Flooding History Matching

Polymer Flooding			
Parameter	History	Simulation	% Difference
Cumulative Liquid, cm^3	162.00	162.00	0.00
Cumulative Oil, cm^3	3.75	3.68	1.99
Cumulative Water, cm^3	158.25	158.32	0.05

Saturation Data from Coreflood:

Initial Water Saturation (*Swi*)	: 0.6350
Initial Oil Saturation (*Soi*)	: 0.3650
Sor @Waterflooding	: 0.2589
Sw @Waterflooding	: 0.7411
Sor @Polymer Flooding (PF)	: 0.2253
Sw @ Polymer Flooding (PF)	: 0.7747

Validation of WF-P History Matching

Water Saturation			
Condition	Lab	Simulation	% Difference
Initial	0.6350	0.6350	0.00
Start of P	0.7411	0.7449	0.51
End of PF	0.7747	0.7782	0.46

Oil Saturation			
Condition	Lab	Simulation	% Difference
Initial	0.3650	0.3650	0.00
Start of P	0.2589	0.2551	1.47
End of PF	0.2253	0.2218	1.57

Figure 4. Results of Coreflood History Match Simulation FP3230S 2000 ppm 1.0 PV Injection

3.1. Polymer Adsorption and Viscosity Analogy

Average crude oil gravity in Zone B was like the average crude oil gravity in Zone A, but the formation brine salinity was significantly different. Therefore, for the polymer to be able to work correctly in Zone B, it would need an adjustment in

JOURNAL OF PETROLEUM AND GEOTHERMAL TECHNOLOGY
ISSN: 2723-0988, e-ISSN: 2723-1496
Vol. 6 No. 2 2025

polymer adsorption and viscosity based on the difference in brine salinity. Figure 5 shows the location and sampling date of reservoir fluids, and Figure 6 shows the comparison of crude oil gravity and formation brine salinity.

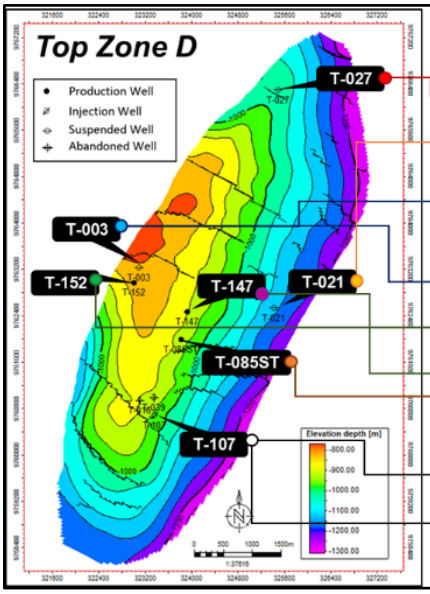

Sampling Date	Well ID	Zone	Interval Test, m	*Salinity, ppm	API Gravity, ^{0}API
30/10/2007	T-027	D	1054.08 - 1056.703	2480	40.73
		C	1075.94 - 1085.09	2480	
08/03/1954	T-021	C	1210 - 1224	2480	40.14
26/02/1956	T-003	A	1024 - 1154	4314	39.98
18/02/1994	T-003	B	965.0 - 992.0	7233	39.8
		A	1025.2 - 1073.8	4314	
04/02/2016	T-152	D	869.5 - 877	2480	40.1
30/10/2007	T-147	B	1064.97 - 1071.07	7233	57.14
		A	1127.76 - 1133.86	4314	
21/11/2008	T-085ST	D	961.99 - 993.98	2480	44.33
05/02/2016	T-107	B	1085.5 - 1120.5	7233	50.9
08/03/1994	T-107	A	1134.2 - 1154.7	4314	40.3

*based on Summary by PEP

Figure 5. Location and Sampling Date of Reservoir Fluids

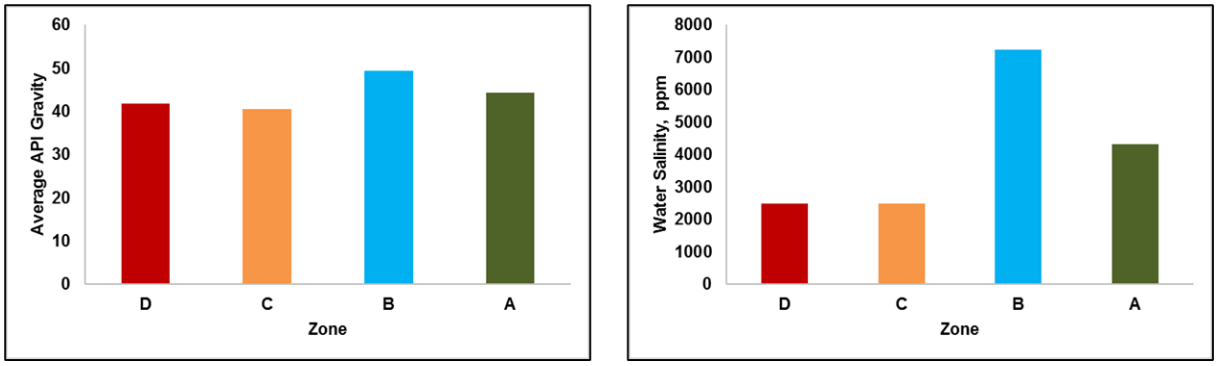

Figure 6. Comparison of Crude Oil Gravity and Formation Brine Salinity

According to Tay, et al. (2015), as the brine salinity in the reservoir increases, chemical adsorption also increases. This indicates that as formation brine salinity becomes higher, the level of chemical adsorption increases, resulting in a longer duration/dwell time required for the chemical saturation process within the rock pores. Results from coreflood lab analysis stated that FP3230S 2000 ppm adsorption level is 1.3303 mg/g of rock sample at brine salinity 4314 ppm. Based on the correlation between salinity and chemical adsorption from the study conducted by Tay, et al (2015), a reconstruction of the relationship between salinity and chemical adsorption was carried out using salinity and chemical adsorption values obtained from Zone A FP3230S 2000 ppm coreflood laboratory test results. Figure 7 shows the correlation between brine salinity and chemical adsorption based on Tay's research, and the reconstructed chemical adsorption versus brine salinity for FP3230S 2000 ppm.

To obtain the adsorption value corresponding to the brine salinity of Zone B which is at 7233 ppm, an extrapolation of the brine salinity versus adsorption correlation was performed. The extrapolation results are shown in Figure 8. Based on this extrapolation, a conversion ratio of the adsorption value for Zone B was obtained as 1.68 times that of Zone A. Using this correction factor, the adsorption value for Zone B was determined to be 2.2305 mg/g of rock sample. The adsorption value for Zone B is listed in Table 2.

Table 2. FP3230S 2000 ppm Adsorption Values for Zone A and Zone B

Zone	Salinity		Adsorption, mg/g
	Parts per million (ppm)	Gram per Liter (g/L)	
A	4314	4.31	1.3303
B	7233	7.22	2.2305

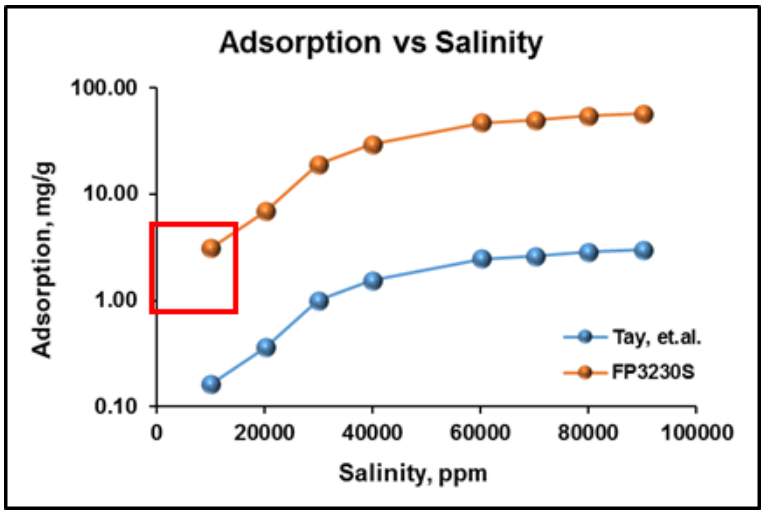

Figure 7. Brine Salinity vs FP3230S 2000 ppm & Reference Chemical Adsorption

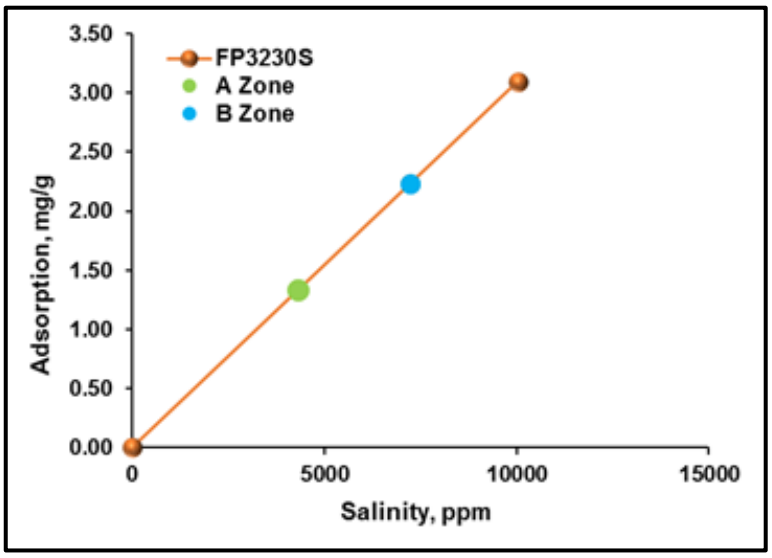

Figure 8. Extrapolation of Brine Salinity vs FP3230S Adsorption Values for Zone A and Zone B

According to Yerramilli, et al. (2013), as the brine salinity in the reservoir increases, chemical viscosity would diminish. This indicates that as formation brine salinity becomes higher, chemical viscosity decreases; thus, increases displacing fluid mobility ratio and would impair sweep efficiency and mobility control features from the displacing fluid. Figure 9 shows the correlation between shear rate and polymer viscosity on various brine salinity based on Yerramilli's research, and by using the trendline for each salinity variation, the polymer viscosity values at 3 salinity variations can be obtained at a shear rate of 7 s^{-1}. Figure 10 also shows an overlay of the polymer viscosity test results for FP3230S in Zone A, which is 15.17 cP at a salinity of 4314 ppm. A reconstruction of the correlation between salinity and polymer viscosity was then carried out using the salinity and polymer viscosity values of FP3230S 2000 ppm in Zone A to determine the polymer viscosity of FP3230S 2000 ppm at the brine salinity of Zone B, which is 7233 ppm. Based on the reconstruction results, a correction factor for polymer viscosity in Zone B was obtained as 0.8847 times the polymer viscosity in Zone A, resulting in a polymer viscosity of FP3230S 2000 ppm for Zone B of 13.42 cP. The polymer viscosity value for FP3230S 2000 ppm in Zone B is listed in Table 3.

Table 3. FP3230S 2000 ppm Viscosity for Zone A and Zone B

Zone	Salinity		Polymer Viscosity, cP
	Parts per million (ppm)	Gram per Liter (g/L)	
A	4314	4.31	15.17
B	7233	7.22	13.42

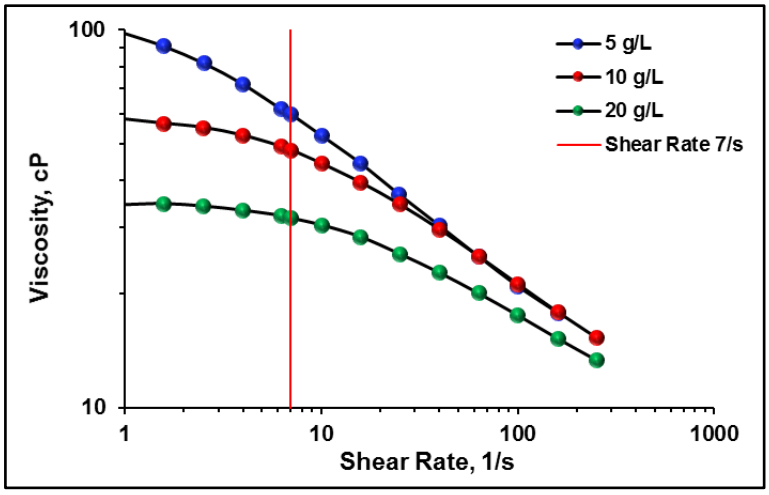

Figure 9. Viscosity at Shear Rate 7 s^{-1} on Various Brine Salinity

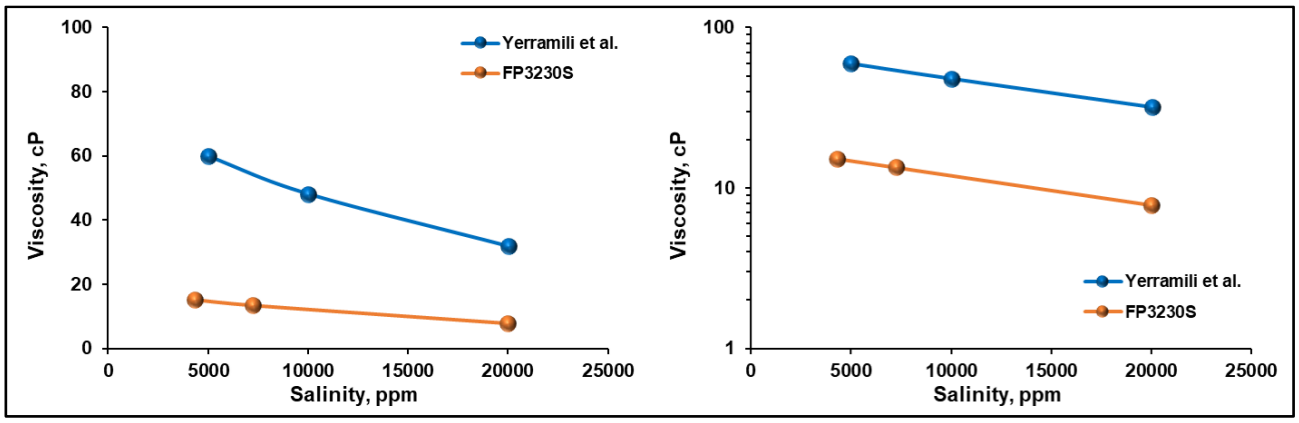

Figure 10. Brine Salinity vs Reference Chemical and FP3230S Viscosity at Shear Rate 7 s^{-1}

3.2. Waterflooding Optimization

Waterflood optimization was performed in two stages: optimization of the flood pattern design and sensitivity analysis of injection operations to injection rate and injection pressure. The waterflooding scheme employed a normal irregular five, six, and seven-spot pattern, with each pattern utilizing one producer as a monitoring well. The selection of injection wells and monitoring production wells for each waterflood pattern was based on the distribution of movable oil saturation at the end of the history-matching period in June 2022, to identify areas with remaining potential for increased oil recovery. Active production and injection wells at the end of the history-matching period, along with the reactivation of suspended injection wells in areas with high movable oil saturation, and the addition of five new injection wells, were implemented to optimize oil recovery in unswept areas. Wells located outside areas of high movable oil saturation were shut in. The total number of injection wells was 24, and the number of monitoring production wells was 10. The injection pattern is shown in Figure 11.

Injection operation sensitivity was evaluated by varying injection rates based on a fluid injected versus fluid produced balance (FIFO), as well as by assessing sensitivity to injection pressure. The baseline waterflood rate for Zone B was 7200 STB/D using 24 injection wells (300 STB/D per well) and was balanced with a Zone B liquid production rate of 7400 STB/D using 10 production wells (740 STB/D per well). Injection rates were varied at 300, 240, 200, 125, and 100 STB/D per well to assess their impact on production performance (Figure 12).

At the lowest injection rate of 100 STB/D per well (total injection 2400 STB/D) under a total liquid production constraint of 3000 STB/D, the liquid production rate was unstable. Reservoir pressure declined to approximately 400 psi, which was insufficient to sustain liquid flow, resulting in a significant reduction in production rate. This indicates that low injection rates are ineffective in maintaining reservoir drive and production performance in Zone B. The optimum injection rate was determined from cumulative oil production using the creaming curve (Figure 13) and was identified as 125 STB/D. This rate provided more stable production throughout the forecast period compared to other injection rate scenarios.

Sensitivity analysis further showed that higher injection rates lead to higher peak oil production during the early stages of the forecast; however, peak production from rates of 200–300 STB/D exceeded the historical secondary peak oil production, suggesting limited long-term benefit from very high injection rates. Following determination of the optimum injection rate, sensitivity to injection pressure was evaluated while ensuring the pressure did not exceed the formation fracture pressure of 2300 psi. Injection pressure was varied from 2000 to 2200 psi (Figure 14). The results showed that a 200-psi variation had no impact on oil production performance, including oil rate, cumulative production, and reservoir pressure. Consequently, the optimum injection pressure was selected as the lowest tested value, 2000 psi.

The optimum waterflooding scenario for Zone B of Field X employed an injection rate of 125 STB/D per injection well at an injection pressure of 2,000 psi. The total liquid production constraint was set equal to the total injection rate of 3,000 STB/D to achieve a fluid injected versus fluid produced balance (FIFO = 1), with 125 STB/D allocated to 24 injection wells and a liquid production constraint of 300 STB/D for 10 production wells. This optimum waterflooding scenario serves as the basis for designing the subsequent polymer injection scenario. A comparison of the base case and the optimum waterflooding scenario is presented in Fig. 15.

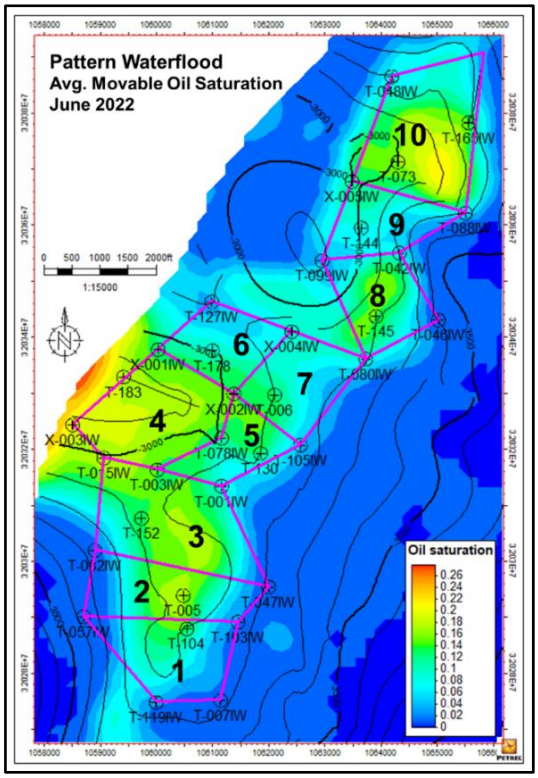

Figure 11. Movable Oil Saturation Map overlaid with Injection Pattern

JOURNAL OF PETROLEUM AND GEOTHERMAL TECHNOLOGY
ISSN: 2723-0988, e-ISSN: 2723-1496
Vol. 6 No. 2 2025

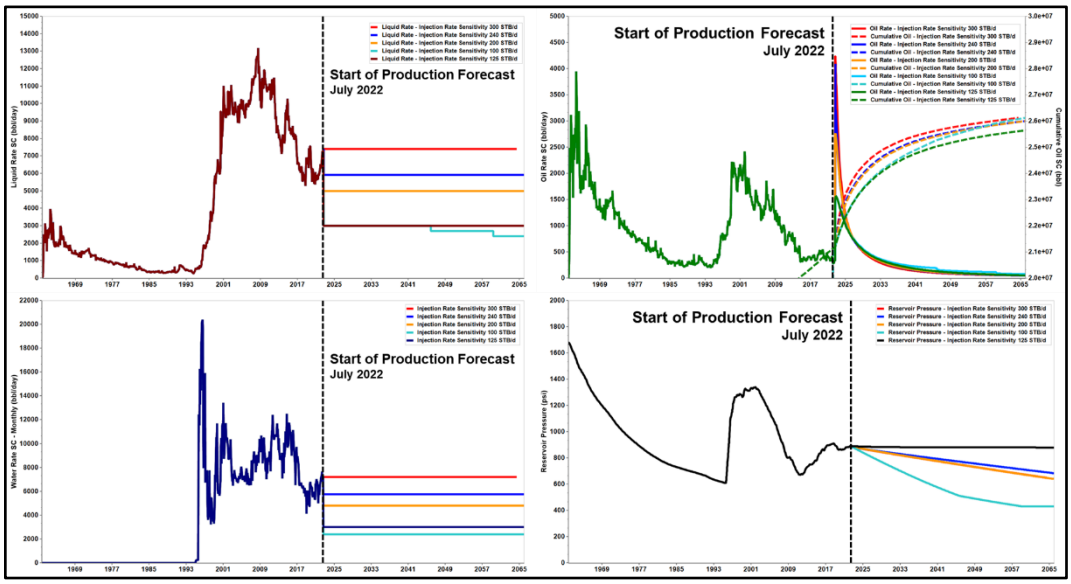

Figure 12. Waterflood Injection Rate Sensitivity Results

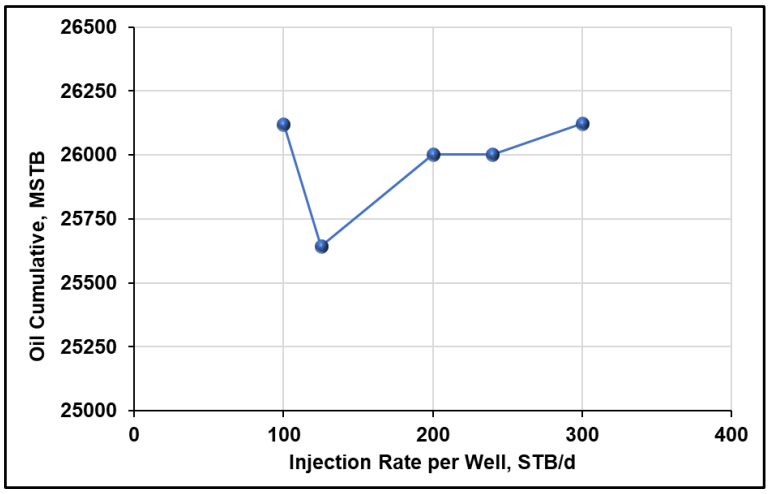

Figure 13. Oil Cumulative Creaming Curve vs Waterflood Injection Rate Sensitivity

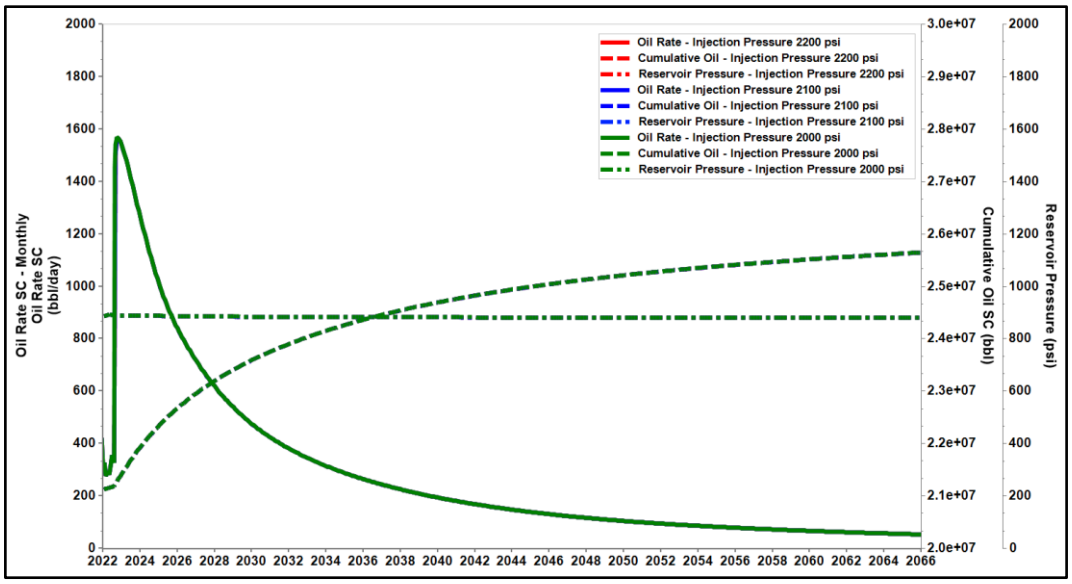

Figure 14. Waterflood Injection Pressure Sensitivity Results

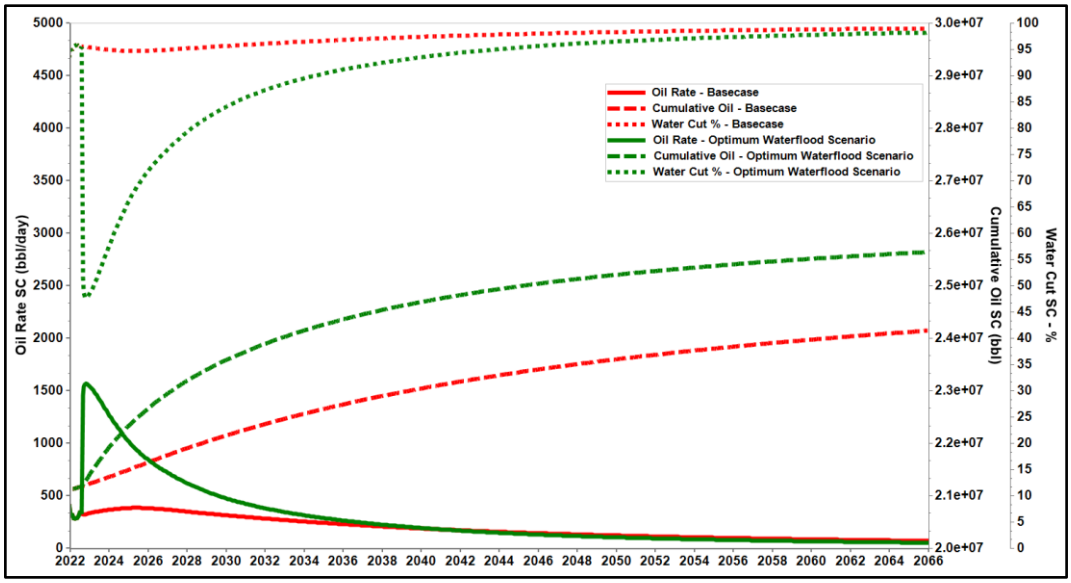

Figure 15. Oil Production Performance at Optimum Waterflooding Scenario

3.3. Polymer Flooding

After the optimum waterflood operational conditions were established, an assessment of polymer flooding application in Zone B was conducted. The assessment process consisted of a screening stage based on established screening criteria, followed by an analysis of reservoir properties to determine patterns that could be prioritized as pilot areas for the optimum polymer injection scenario in Zone B. The pattern analysis criteria, based on Taber et al. (1996), Dong et al. (2008), and Liang et al. (2018), are presented in Figure 16.

Polymer			
	Criteria	Weight	Preferable Conditions
I	Movable Oil Saturation	10	The higher the better [1], has the same weight to Permeability
II	Movable Remaining Oil in Place	20	The higher the better [1], function of Oil Saturation, Area, Thickness, Porosity. Has 2x weight to Oil Saturation and Permeability [2]
III	Area Pattern	10	The smaller the better [3], function of Well Spacing. Well Pattern has small effect to incremental recovery [3]
IV	Average Transmissibility	10	The higher the better [1], function of Permeability and Thickness, has the same weight to Oil Saturation

References:

1. Taber, et. al., 1996. *EOR Screening Criteria Revisited – Part 1: Introduction to Screening Criteria and Enhanced Oil Recovery Field Projects*. doi: 10.2118/35385-PA
2. Liang, et. al., 2018. *Novel Enhanced-Oil-Recovery Decision-Making Workflow Derived From the Delphi-AHP-TOPSIS Method: A Case Study*. doi: 10.2118/176444-PA
3. Dong, et. al., 2008. *Review of Practical Experience & Management by Polymer Flooding at Daqing*. doi: 10.2118/114342-MS

Figure 16. Weighted Injection Pattern Screening Criteria

The post-waterflood reservoir rock properties of Zone B were evaluated to assess the suitability of polymer flooding, with porosity and movable remaining oil saturation used to represent the movable remaining oil in place, and permeability used to indicate rock transmissibility within each pattern. From the initial set of 10 candidate injection patterns, Pattern 4 and Pattern 5 (Figure 11) were excluded from further consideration as they were intersected by major fault line. As reported by Dong et al. (2008), patterns intersected by major faults are not favorable for polymer injection due to potential flow discontinuities and reduced sweep efficiency. Consequently, these two patterns were not considered in the prioritization process. Based on the remaining patterns and the applied screening criteria, Pattern 6 emerged as the most suitable pilot area for conducting optimum polymer injection sensitivity analysis.

Pattern 6 in Zone B (Figure 18) was selected as the pilot area and exhibits an average porosity of 11.15%, an average permeability of 220.74 mD, and a post-waterflood movable remaining oil saturation of 0.0259. The porosity–permeability relationship indicates that Pattern 6 is predominantly composed with moderate-to-good flow capacity due to great reservoir thickness. The permeability range of approximately 200 mD observed in Pattern 6 is consistent with that of the stacked native coreflood samples, suggesting that the pilot pattern model is representative of laboratory-scale flow

behavior. This similarity supports the applicability of polymer flooding performance observed in coreflood experiments to field-scale conditions. The selection of Pattern 6 as the pilot polymer injection pattern was further justified by the comparable porosity–permeability distribution, the relatively smallest areal extent—allowing improved operational control—and the presence of remaining movable oil after waterflooding. Collectively, these characteristics indicate favorable conditions for mobility control improvement and incremental oil recovery through polymer flooding.

Following completion of the assessment process and pilot area selection, sensitivity analyses on injection rate and injection pressure were conducted to identify the optimum polymer injection scenario. The first polymer injection sensitivity focused on the effect of injection and production rate variations while maintaining a fluid-injected versus fluid-produced (FIFO) balance. This approach ensured volumetric consistency, minimized reservoir pressure distortion, and isolated the impact of polymer mobility control on sweep efficiency. Polymer injection rates were varied at 200, 175, 125, 100, 75, and 50 STB/D per injection well, while total liquid production rates were adjusted to remain balanced with the total injection rate. Pattern 4 and Pattern 5 were maintained under optimum waterflood conditions and excluded from the polymer injection sensitivity analyses.

As shown in Figure 19, the polymer injection rate sensitivity analysis demonstrates that higher injection rates lead to greater incremental oil production. This trend is attributed to the simultaneous adjustment of liquid production rates per producer well, balanced with the increased injection rates. The optimum polymer injection rate was determined by evaluating the creaming curve of cumulative oil production on Figure 20, identifying 200 STB/D per injection well as the preferred rate. At this rate, the highest oil gain was achieved, while the production decline during the polymer injection period remained comparable to other rate sensitivity scenarios. These results indicate that higher injection rates enhance sweep efficiency without adversely affecting reservoir performance or well operation.

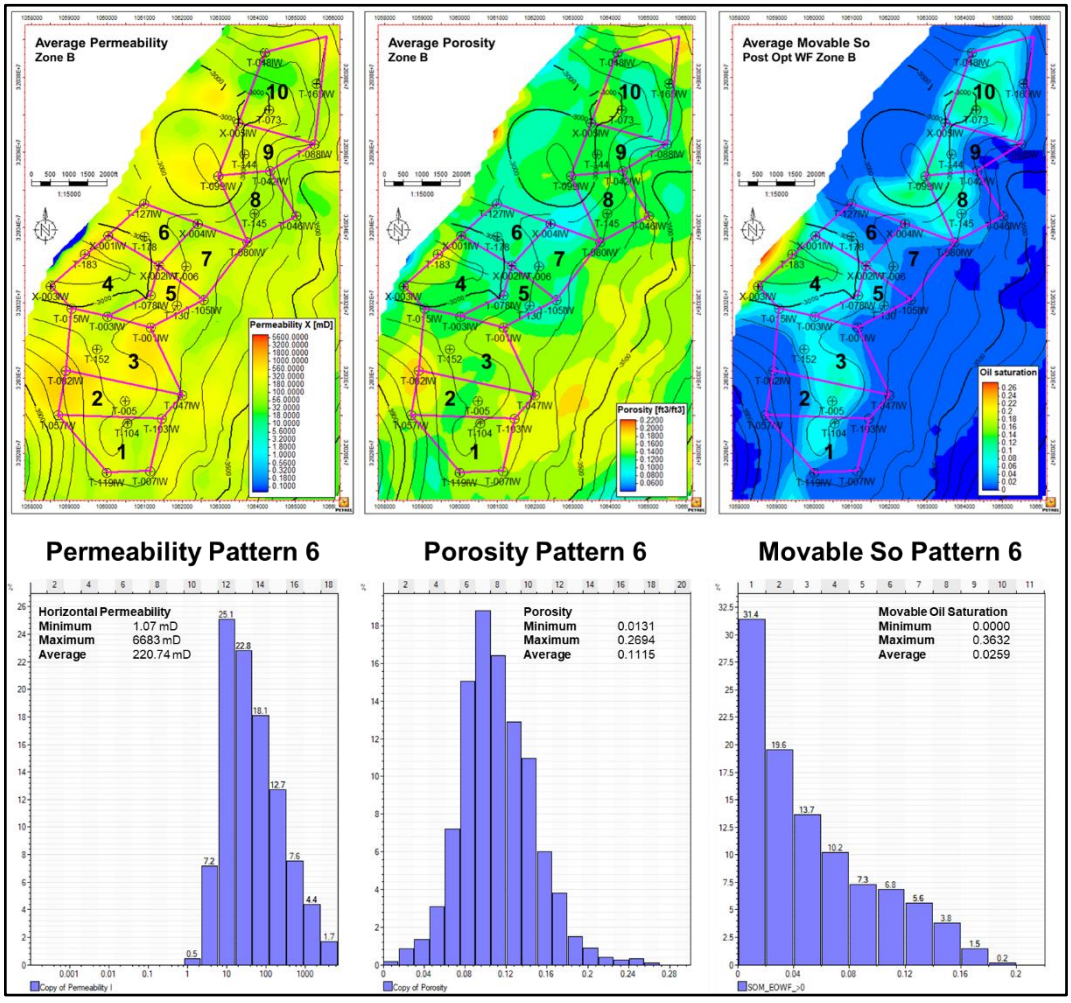

Figure 18. Distribution and Histogram of Porosity, Permeability, and Movable Oil Saturation Post-Waterflood

Following determination of the optimum polymer injection rate, sensitivity analyses were conducted on injection pressure, varied from 2000 to 2200 psi, while remaining below the formation fracture pressure of 2300 psi. The results (Figure 21)

indicate that injection pressure variations within this range have no impact on oil production performance, be it oil production rate gain, nor cumulative oil production gain. Consequently, the optimum injection pressure for polymer flooding was selected as 2200 psi, accommodating the higher viscosity of the polymer solution relative to waterflooding without compromising formation integrity or reservoir performance.

Having identified the optimum polymer injection rate and pressure, the next step was to evaluate the spatial impact of polymer flooding on reservoir flow behavior. Flow vector and water sweep streamline analyses provide insight into the distribution of injected polymer and the resulting improvement in oil displacement, allowing visualization of sweep efficiency enhancements under the selected operational conditions.

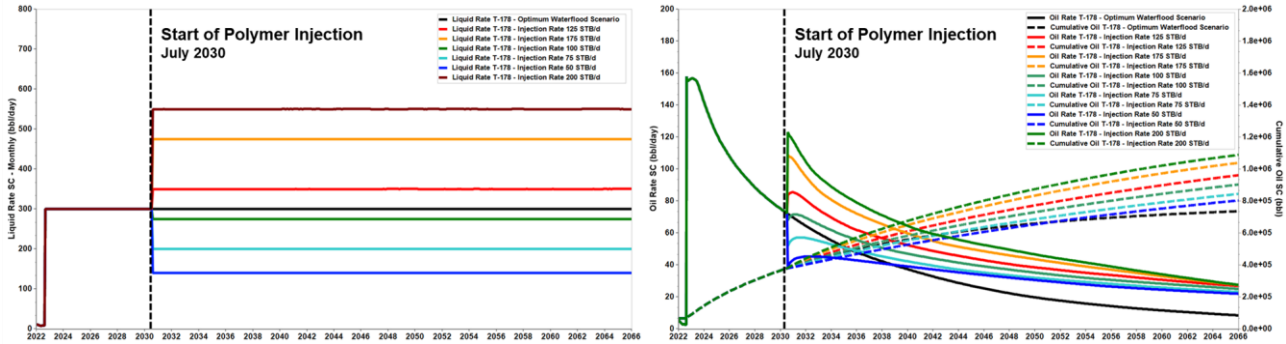

Figure 19. Pattern 6 Production Performance on Various Polymer Injection Rate Sensitivity

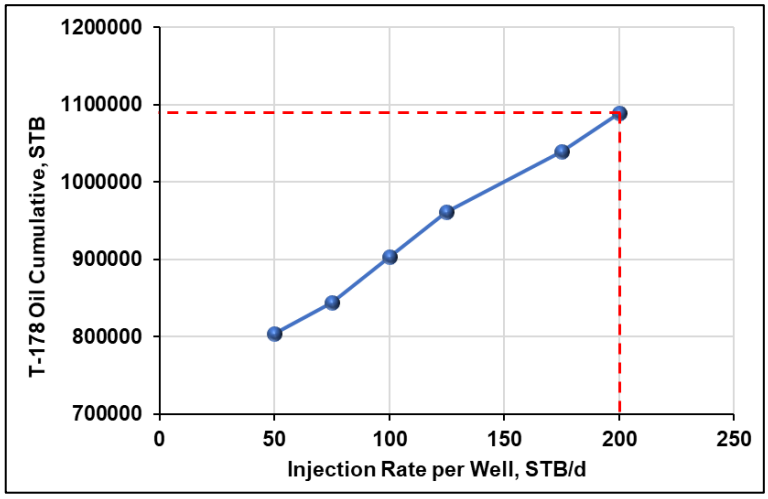

Figure 20. Pattern 6 Oil Cumulative Creaming Curve on Various Polymer Injection Rate

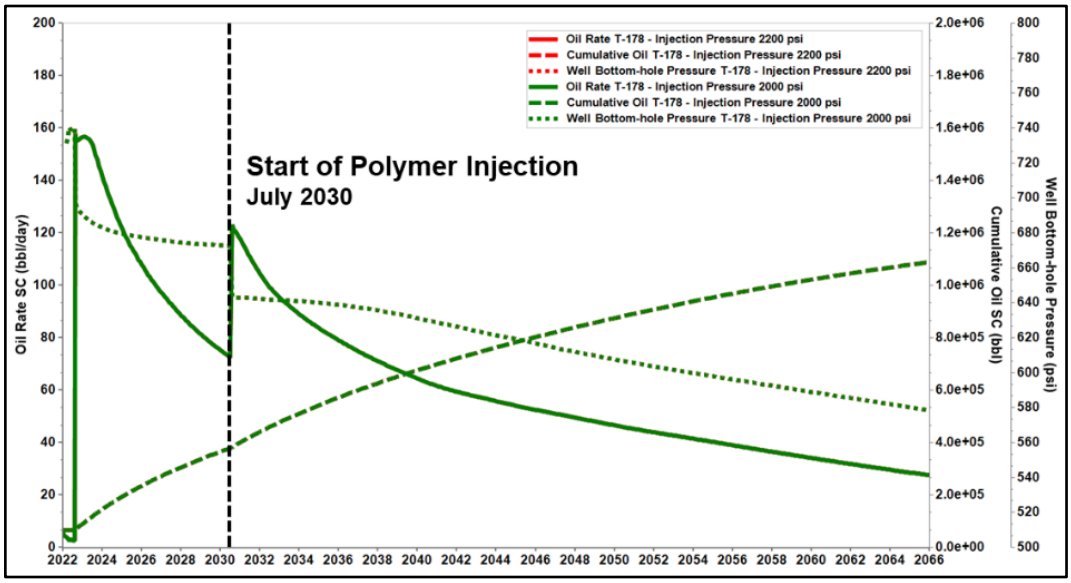

Figure 21. Pattern 6 Production Performance on Various Polymer Injection Pressure Sensitivity

As shown in Figure 22, differences in the injection fluid flow vectors, representing flow intensity, are observed between the end of the waterflood scenario in July 2030 and the conditions in August 2030 following polymer injection into the reservoir. Figure 22 also further illustrates variations in oil flow vectors, reflecting both flow intensity and oil recovery, as well as changes in water sweep streamlines, which indicate the displacement direction of the injected fluid. These comparisons reveal an improvement in oil recovery and sweep efficiency within Pattern 6 after polymer injection, highlighting the positive impact of polymer flooding on reservoir displacement performance.

Based on Table 4, oil production under the optimum waterflood and polymer injection scenarios for Pattern 6 at the end of the production forecast in January 2066 demonstrates an incremental recovery factor of 16.71% relative to the optimum waterflood scenario. This incremental recovery exceeds that observed in coreflood experiments, confirming that polymer injection enhances sweep efficiency beyond the immediate injection wells in Pattern 6. The process forms an oil bank, supplying residual oil within Pattern 6 that is produced by the monitoring well T-178, and its effect is further amplified by the operational difference in injection rates between the waterflood and polymer flooding periods.

Table 4. Pilot Pattern 6 Production Forecast Results

Scenario	OOIP, MSTB	June 2022		January 2066		Increment	
		Np MSTB	RF %	Np MSTB	RF %	Np MSTB	RF %
Base Case	**2109.33**	89.59	4.25	91.20	4.32	-	-
BC + Opt. WF				759.04	35.99	667.85	31.66
BC + Opt. WF & Polymer				1111.50	52.69	352.46	16.71

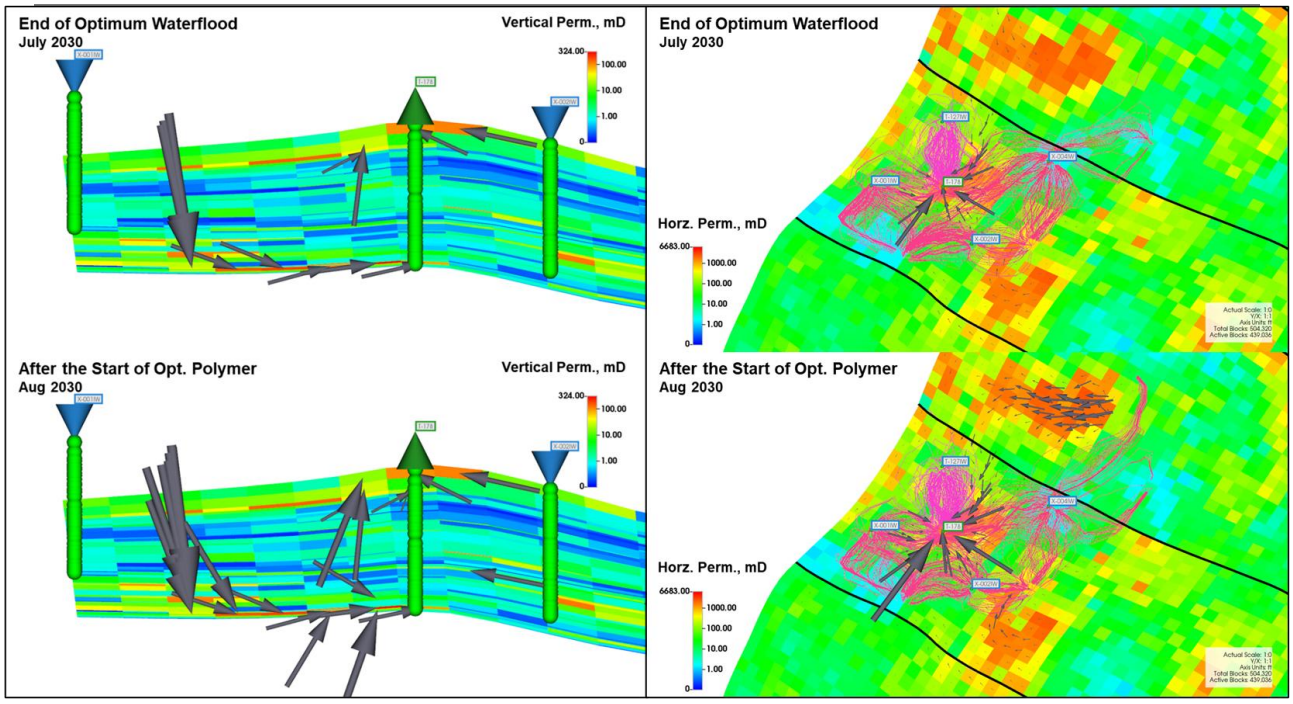

Figure 22. Pattern 6 Oil Cumulative Creaming Curve on Various Polymer Injection Rate

The full-field implementation of the optimum injection scenario combines the results of the optimum waterflood and pilot-area polymer injection strategies. The polymer injection start date was determined based on the breakthrough phase identified from the water saturation versus water fractional flow/water cut curve (Figure 23), which indicates that Zone B of Field X enters breakthrough at a water cut of 85%. Under the optimized waterflood scenario, this threshold is reached in July 2030, establishing the polymer injection start date. The waterflood phase uses an injection rate of 125 STB/D per well at 2000 psi, while the polymer injection phase employs 200 STB/D per well at 2200 psi. Patterns 4 and 5 remain under the optimized waterflood scenario.

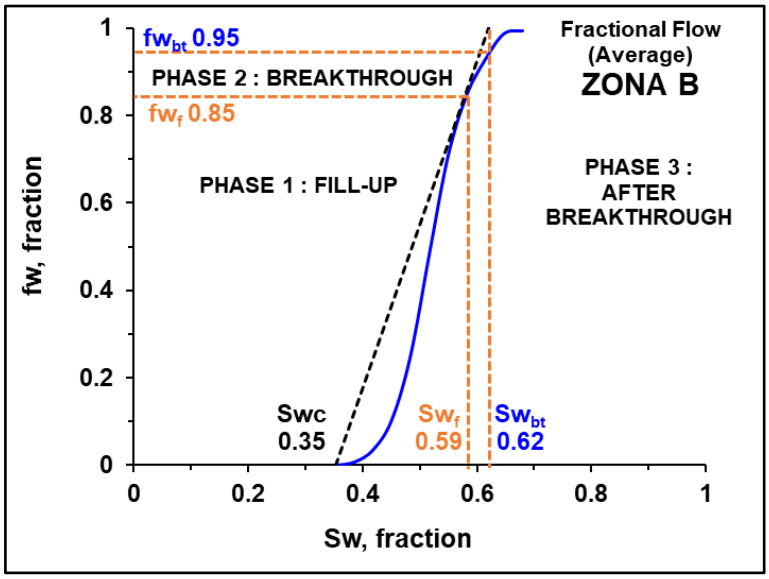

Figure 23. Pattern 6 Oil Cumulative Creaming Curve on Various Polymer Injection Rate

Figure 24 shows that the initial polymer injection period exhibits a clear alteration in water cut profiles, demonstrating the effect of polymer as a mobility control fluid and its role in improving sweep efficiency. At the end of the production forecast in January 2066, this combined scenario yields an incremental recovery factor of 3.13% relative to the base case. While this incremental recovery is smaller than that observed in the pilot-area analysis—since the oil bank is now simultaneously distributed across all patterns and produced by their respective monitoring wells—it nonetheless confirms that polymer injection effectively enhances sweep efficiency across all target patterns, forming oil banks that contribute to increased overall oil recovery, which further justified in Figure 25. Production forecast results can be seen in Table 5

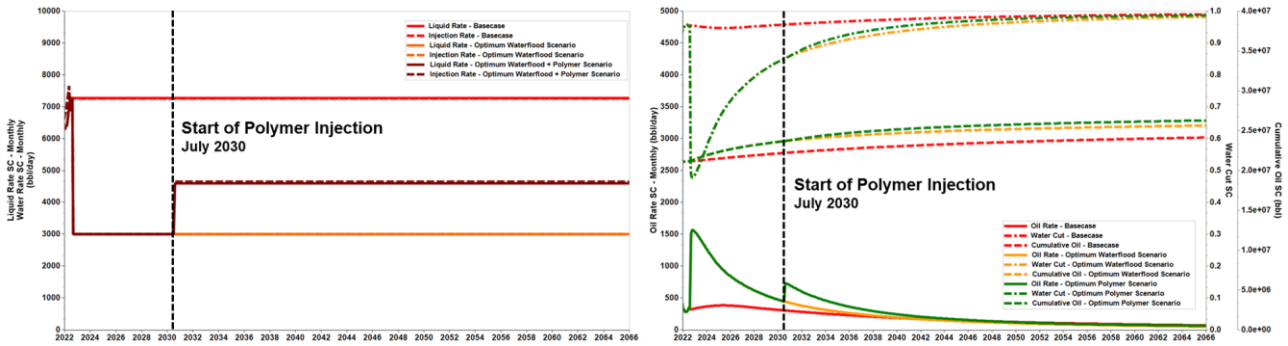

Figure 24. Base-Case and Full-scale Optimization Scenario Oil Production Performance

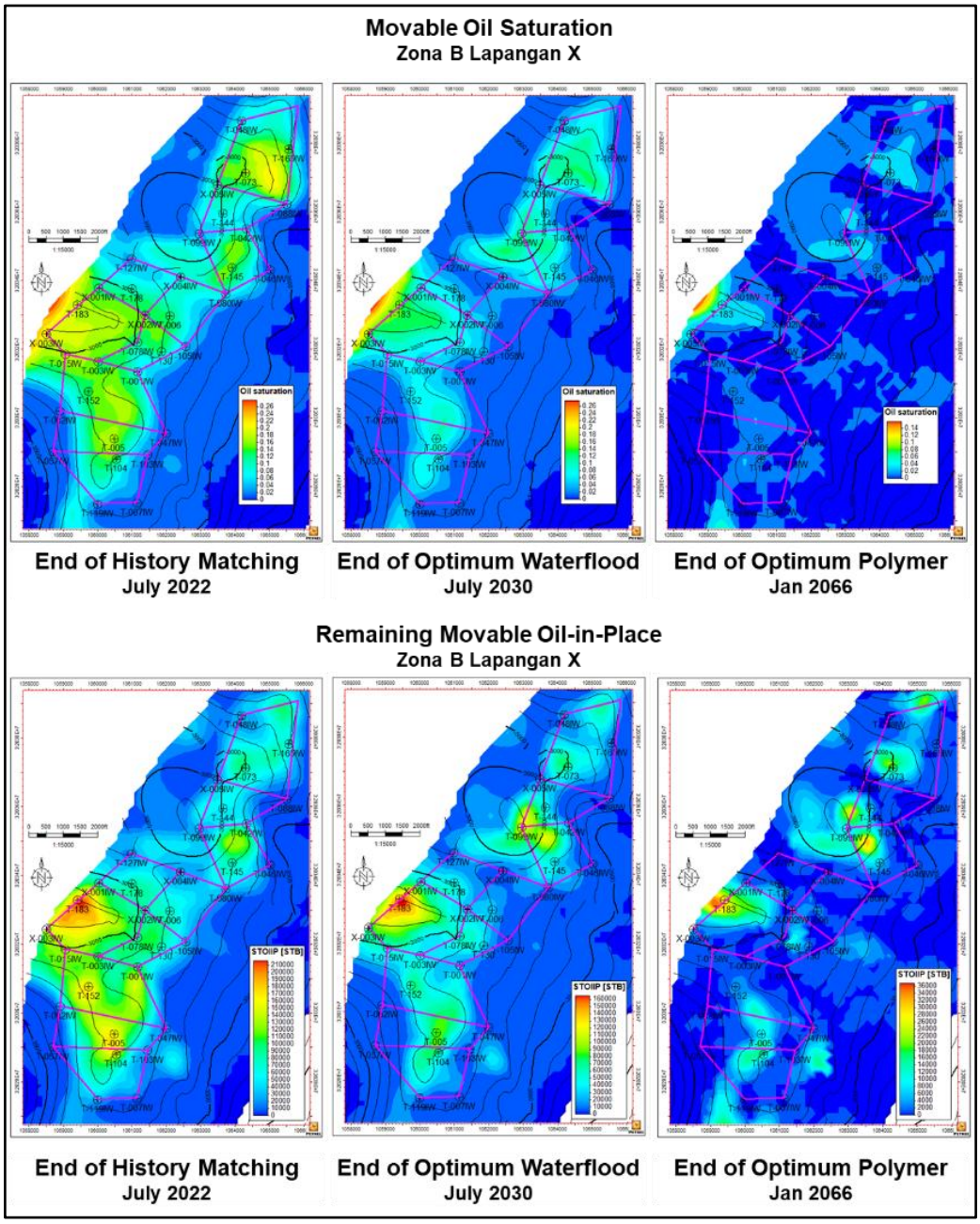

Figure 25. Optimization Scenario Movable Oil Saturation and Remaining Movable Oil-in-Place Distribution

Table 5. Zone B of Field X Production Forecast Results

Scenario	OOIP, MMSTB	June 2022		January 2066		Increment	
		Np, MMSTB	RF %	Np, MMSTB	RF %	Np, MMSTB	RF %
Base Case	**68.35**	22.16	32.42	24.15	35.33	-	-
BC + Opt. WF				25.64	37.52	1.50	2.19
BC + Opt. WF & Polymer				26.29	38.46	2.14	3.13

IV. CONCLUSION

Several conclusions are made to summarize this study:

1. Zone B exhibits 16% porosity, 14.21 mD permeability, 33% connate water saturation, and 28% residual oil, with 84 production wells and 22 injection wells.

2. Pattern 6 was selected as the polymer pilot area due to favorable porosity–permeability, residual oil, minimal area, reservoir high location, and near-square geometry. Pattern selection also changed the total active wells for production forecast.
3. Waterflood begins in July 2022, then full-field polymer injection commenced in July 2030, combining optimum waterflood (125 STB/D per well, 2000 psi) with polymer injection (200 STB/D per well, 2200 psi), maintaining FIFO balance. By January 2066, waterflood produced 1.5 MMSTB incremental oil gain (2.19% incremental RF), and polymer flooding added 2.14 MMSTB (3.13% incremental RF), improving sweep efficiency and mobilizing residual oil.

ACKNOWLEDGEMENTS

This work was supported by Universitas Pembangunan Nasional "Veteran" Yogyakarta and Widyasarana Consulting and Engineering. The authors acknowledge all the support that has been given during research, publication, and presented this paper. Writer would kindly appreciate any input and recommendations.

REFERENCES

Al-Murayri, M.T., et al. (2019), Chemical EOR Pilot Design Optimization Through Dynamic Reservoir Characterization. *SPE Kuwait Oil & Gas Conference and Show*. https://doi.org/10.2118/198035-ms

Dong, H.Z. (2008). Review of Practical Experience & Management by Polymer Flooding at Daqing. *SPE/DOE Improved Oil Recovery Symposium*. https://doi.org/10.2118/114342

Ghadami, N., et al. (2016), Robust Chemical EOR Modelling from Coreflood to Full Field Scale in a Brown Field, Offshore. *SPE Asia Pacific Oil & Gas Conference and Exhibition*. https://doi.org/10.2118/182376-ms

Hatzignatiou, D.G., et al. (2013), Experimental Investigation of Polymer Flow through Water- and Oil-Wet Berea Sandstone Core Samples. *SPE Europec/EAGE Annual Conference and Exhibition*. https://doi.org/10.2118/164844

Hazarika, K., et al. (2022), Polymer Flooding and Its Effects on Enhanced Oil Recovery: Upper Assam Basin. *Petroleum Research 8 – 2023 (54-62)*. https://doi.org/10.1016/j.ptlrs.2022.03.003

Liang, Bin, et al. (2015), Novel Enhanced Oil Recovery Decision Making Workflow Derived from the Delphi-AHP-TOPSIS Method: A Case Study. *SPE/IATMI Asia Pacific Oil & Gas Exhibition*. https://doi.org/10.2118/176444-pa

Najafabadi, N.F., et al. (2016), Proper Simulation of Chemical EOR (CEOR) Pilots – A Case Study. *SPE Improved Oil Recovery Conference*. https://doi.org/10.2118/179659-ms

Pandey, A., et al. (2008), Chemical Flood Simulation of Laboratory Corefloods for the Mangala Field: Generating Parameters for Field-Scale Simulation. *SPE/DOE Improved Oil Recovery Symposium*. https://doi.org/10.2118/113347

Taber, J.J., et al. (1997), EOR Screening Criteria Revisited – Part 1: Introduction to Screening Criteria and Enhanced Recovery Field Projects. *SPE Improved Oil Recovery Symposium*. https://doi.org/10.2118/35385-pa

Tay, A., et al. (2015), Adsorption Inhibitors: A New Route to Mitigate Adsorption in Chemical EOR. *SPE Enhanced Oil Recovery Conference*. https://doi.org/10.2118/174603-ms

Yerramilli, S.S., et al. (2013), Novel Insight into Polymer Injectivity for Polymer Flooding. *SPE European Formation Damage Conference and Exhibition*. https://doi.org/10.2118/165195